Volume 11
Number 4
April 2026
Pages 919–1164

Nanoscale Horizons

The home for rapid reports of exceptional significance in nanoscience and nanotechnology

rsc.li/nanoscale-horizons

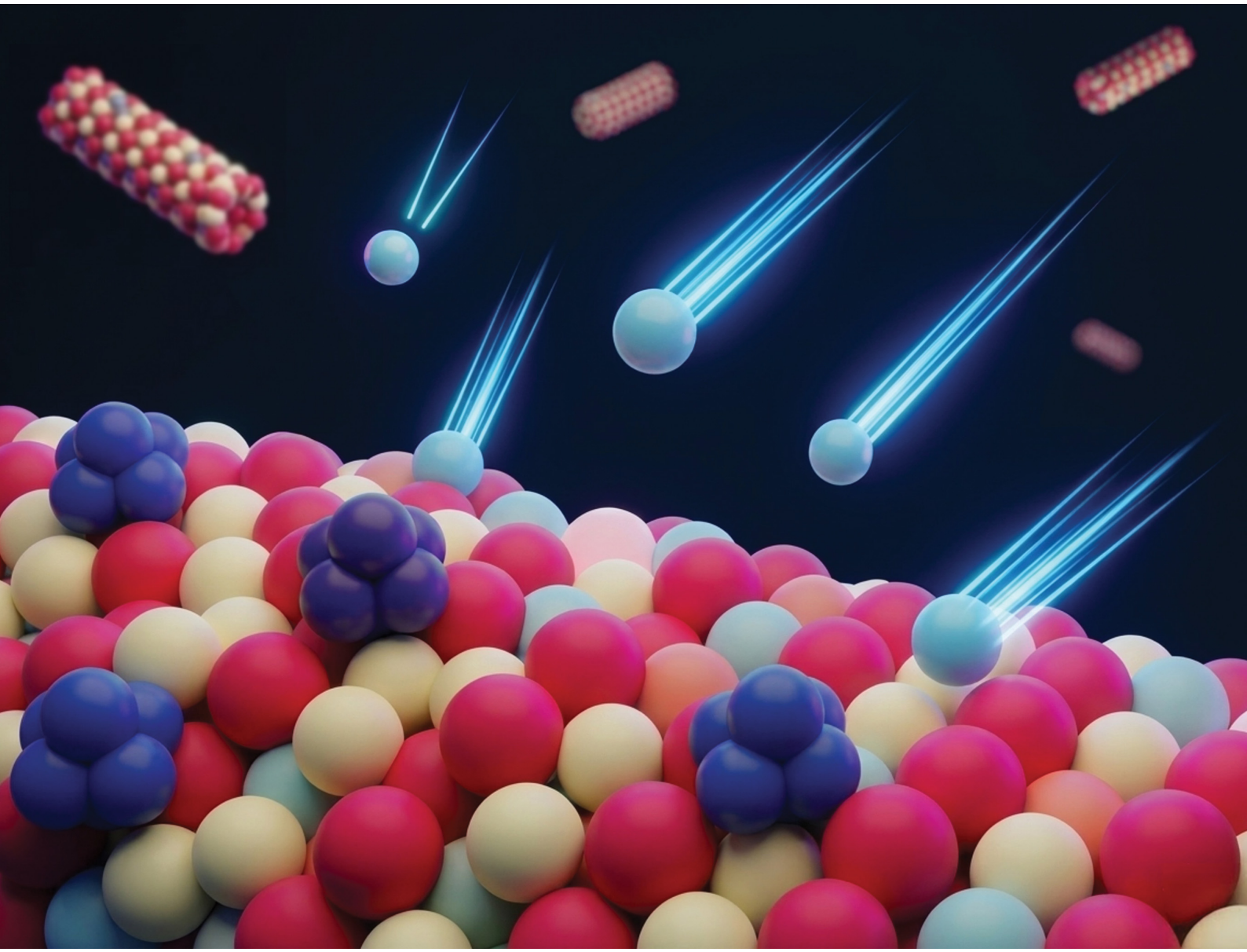

ISSN 2055-6756

ROYAL SOCIETY OF CHEMISTRY

COMMUNICATION

Youngran Seo, Dongwon Yoo *et al.*

Tunable rhenium–ceria–zirconia catalysts for efficient deoxydehydration of C_6 polyols: lattice engineering enables high muconate yield

NCNST

Nanoscale Horizons

ROYAL SOCIETY OF CHEMISTRY

COMMUNICATION

View Article Online
View Journal | View Issue

Check for updates

Cite this: *Nanoscale Horiz.*, 2026, **11**, 1006

Received 16th December 2025,
Accepted 4th March 2026

DOI: 10.1039/d5nh00816f

rsc.li/nanoscale-horizons

Tunable rhenium–ceria–zirconia catalysts for efficient deoxydehydration of C_6 polyols: lattice engineering enables high muconate yield

Guk Hee Yim,†[a] Hyunwoo Choi,†[a] Hyeonjeong Son,†[a] Juhye Park,[a] Ahyun Jeon,[a] Youngran Seo *[a] and Dongwon Yoo *[ab]

Sustainable routes to adipic acid from biomass-derived C_6 polyols typically rely on a two-step deoxydehydration (DODH)–hydrogenation sequence, of which the DODH step remains the primary barrier to industrial adoption. Here, we report a tunable rhenium catalyst supported on ceria–zirconia mixed oxides ($Re/Ce_xZr_{1-x}O_2$) engineered through precise control of metal-support interactions. Thermal diffusion of Zr^{4+} into CeO_2 nanorods induces lattice contraction and elevates the Ce^{3+} fraction, substantially enhancing the reducibility of surface rhenium species and accelerating the rate-determining step in Re-catalyzed DODH. Remarkably, up to 70 at% Zr can be incorporated without structural degradation, providing an unprecedented combination of oxygen mobility and rhenium redox synergy. The optimized $Re/Ce_{0.3}Zr_{0.7}O_2$ catalyst delivers *trans, trans*-muconate in 93% yield from galactarate using *n*-butanol, which functions simultaneously as solvent and green reductant.

New concepts

This work introduces a lattice-engineering strategy that unlocks the full catalytic potential of rhenium-based deoxydehydration (DODH) by precisely tuning the reducibility of ceria–zirconia mixed oxides at the nanoscale. Rather than modifying the active metal itself, we demonstrate that controlled Zr^{4+} diffusion into CeO_2 nanorods contracts the oxide lattice and elevates the Ce^{3+} population, creating an oxygen-vacancy-rich support that dramatically accelerates the turnover-limiting $Re^{6+} \rightarrow Re^{4+}$ reduction step during catalysis. Distinct from prior DODH studies that focus on rhenium speciation, ligand design, or reaction conditions, this work establishes the support lattice as an active kinetic regulator. Importantly, we reveal that excessive Zr incorporation disrupts solid-solution behavior, inducing lattice relaxation and phase segregation that reverses catalytic benefits—highlighting a previously unrecognized composition-structure-reactivity boundary in Ce–Zr oxides. The key insight is that oxide lattice compressibility and redox flexibility can be rationally programmed through nanoscale compositional tuning, enabling dynamic regeneration of active metal sites under reaction conditions. This principle provides a broadly applicable framework for designing next-generation heterogeneous catalysts in biomass upgrading and redox-driven transformations, where catalyst regeneration—not intrinsic activity—limits performance.

Introduction

Adipic acid (hexanedioic acid) is a key monomer for nylon-66, polyesters, and plasticizers, with a global annual demand exceeding 3.5 million tons.[1–4] Conventional production from ketone-alcohol (KA) oil *via* nitric acid oxidation generates substantial nitrous oxide (N_2O), a long-lived greenhouse gas, highlighting the urgent need for greener synthetic routes.[5–7] In this context, catalytic valorization of lignocellulosic carbohydrates has emerged as a promising alternative, enabling the conversion of C_6 sugars and polyols into 1,6-dicarboxylic acids that can be transformed into adipic acid through a sequential deoxydehydration (DODH)–hydrogenation pathway.[8–12]

The DODH reaction, which removes vicinal hydroxyl groups to afford olefin intermediates, is typically mediated by rhenium-based catalysts (Fig. 1(a)).[13–19] In heterogeneous systems, the redox and structural properties of the oxide support strongly influence rhenium speciation[20–23] and govern the rate-determining reduction of Re^{6+} to Re^{4+}, a key step that regenerates active sites for catalytic turnover.[21] CeO_2 is a versatile oxide support owing to its intrinsic Ce^{3+}/Ce^{4+} redox flexibility.[24–26] However, this redox flexibility alone is insufficient to efficiently drive polyol DODH or to sustain effective Re redox cycling during catalysis, thereby necessitating additional metal promoters, such as Au nanoparticles.[27–29]

Here, we present a lattice-engineered $Re/Ce_xZr_{1-x}O_2$ nanorod catalyst that achieves highly efficient DODH of biomass-derived C_6 polyols. Controlled thermal diffusion of smaller Zr^{4+} ions into the CeO_2 lattice produced mixed-oxide supports containing up to 70 at% Zr—a substantially high level—while preserving the structure. This extensive Zr incorporation induced lattice contraction

[a] *Department of Chemical and Biological Engineering, and Institute of Chemical Processes, Seoul National University, Seoul 08826, Republic of Korea. E-mail: youngran02@snu.ac.kr, dwyoo@snu.ac.kr*
[b] *Center for Nanoparticle Research, Institute for Basic Science (IBS), Seoul 08826, Republic of Korea*
† These authors contributed equally to this work.

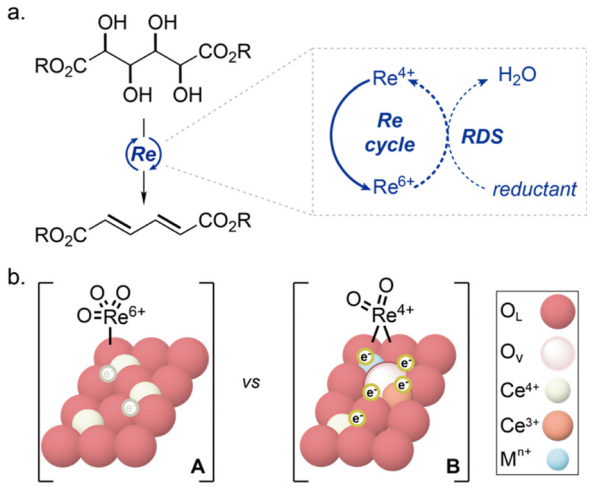

Fig. 1 (a) Rhenium-catalyzed deoxydehydration (DODH) of a biomass–derived C_6 polyol. (b) Schematic illustration of Re species supported on CeO_2 and lattice–modified CeO_2.

and enriched Ce^{3+} sites, thereby enhancing the reducibility of supported Re species (Fig. 1(b)).[30–32] Among the prepared catalysts, $Re/Ce_{0.3}Zr_{0.7}O_2$ exhibited outstanding activity in the DODH of galactarate using *n*-butanol as both solvent and green reductant, delivering *trans*, *trans*-muconate in 93% yield as a single product. Overall, this work demonstrates how nanoscale lattice engineering and oxygen-vacancy modulation in mixed oxides can strengthen metal-support redox synergy, advance rhenium-catalyzed DODH, and contribute sustainable adipic-acid production from renewable carbon sources.

Results and discussion

Zirconium-doped ceria nanorods ($Ce_xZr_{1-x}O_2$) were prepared by thermally incorporating zirconium into preformed CeO_2 nanorods to systematically probe the effects of Zr incorporation within a uniform nanorod framework (Fig. 2(a)). Pristine CeO_2 nanorods were synthesized *via* the hydrothermal treatment of $Ce(NO_3)_3{\cdot}6H_2O$ in 6 M NaOH aqueous solution,[33] followed by post-synthetic Zr diffusion. Defined amounts of $ZrO(NO_3)_2{\cdot}H_2O$ were added to 400 mg of CeO_2 nanorods, treated at 180 °C for 10 h, and subsequently calcined at 600 °C for 6 h in air. The resulting mixed oxides were designated $Ce_{0.5}Zr_{0.5}O_2$, $Ce_{0.3}Zr_{0.7}O_2$, and $Ce_{0.2}Zr_{0.8}O_2$ based on their atomic ratios determined by X-ray photoelectron spectroscopy (XPS) (Fig. 2(b)). As higher amounts of Zr^{4+} were incorporated, the Ce^{3+} (902.3, 898.9, 883.9, 880.6 eV) concentration and oxygen-vacancy (O_V, 531 eV) density both increased, and the nanorod surfaces became rougher, while the overall rod-like morphology maintained intact (Fig. 2(c)–(d) and Fig. S1).

The incorporation of Zr^{4+}, which has a smaller ionic radius (0.84 Å) than Ce^{4+} (0.97 Å), induces local lattice strain and thereby lowers the oxygen-vacancy formation energy.[34–37] As the Zr^{4+} content increases, both the oxygen-vacancy density and Ce^{3+} concentration increase, accompanied by a positive shift of the O 1s XPS peak. This shift originates from the combined

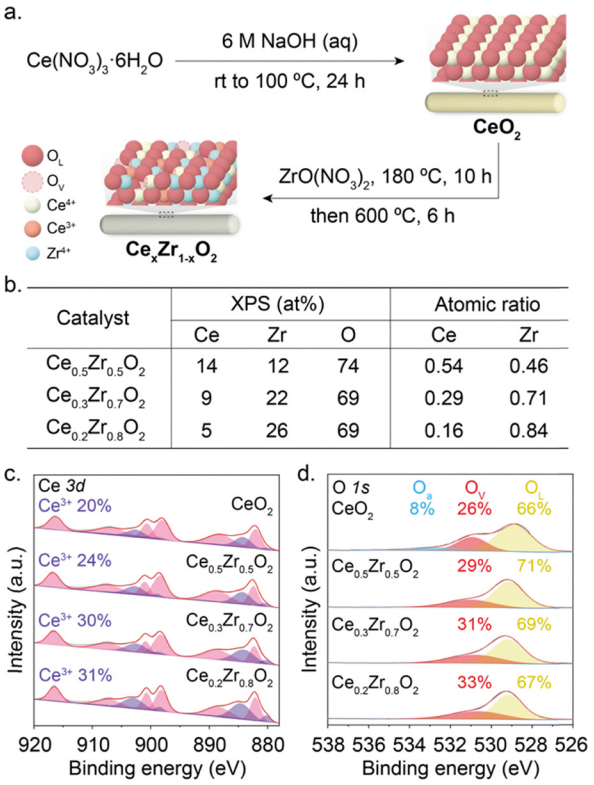

Fig. 2 Preparation for ceria–zirconia nanorods ($Ce_xZr_{1-x}O_2$). (a) Synthetic scheme for $Ce_xZr_{1-x}O_2$ nanorods. (b) XPS-determined Ce/Zr atomic ratios. (c) Ce 3d and (d) O 1s XPS spectra of the mixed oxides.

effects of the higher electronegativity of Zr^{4+} and the partial reduction of ceria (Fig. 2(c) and (d)). The enhanced oxygen-vacancy concentration in $Ce_{0.3}Zr_{0.7}O_2$, compared to bare CeO_2, was further confirmed by electron paramagnetic resonance (EPR) spectroscopy (Fig. S2).[38,39] Consequently, incorporation of the more electronegative Zr^{4+} generates more reducible nanorod supports for Re catalysis, which is also reflected by the systematic shift of the O 1s peak toward higher binding energy (Fig. 2(d)).[40–43]

Rhenium oxide was subsequently impregnated onto pristine CeO_2 and each mixed-oxide support to produce the $Re/Ce_xZr_{1-x}O_2$ catalysts (Fig. 3(a)). The Re loadings, determined by inductively coupled plasma-atomic emission spectroscopy (ICP-AES), were 4.8–5.2 wt% across all samples (Table S1). Transmission electron microscopy (TEM) revealed that their overall rod-like morphology was well preserved after Re impregnation (Fig. 3(b)–(e)). XPS analysis of the $Re/Ce_xZr_{1-x}O_2$ catalysts revealed that the trend of increasing Ce^{3+} concentration and oxygen-vacancy formation with higher Zr^{4+} content is retained after Re impregnation (Fig. 3(f)–(g)). Notably, compared with their corresponding $Ce_xZr_{1-x}O_2$ supports, the $Re/Ce_xZr_{1-x}O_2$ catalysts exhibit further enhanced Ce^{3+} populations and oxygen-vacancy densities. Although charge transfer from Re to the oxide support would typically shift the O 1s XPS peak toward lower binding energy,[44] the O 1s XPS of $Re/Ce_xZr_{1-x}O_2$ instead show a positive binding energy shift. This behavior can be explained by electron back-donation from the highly

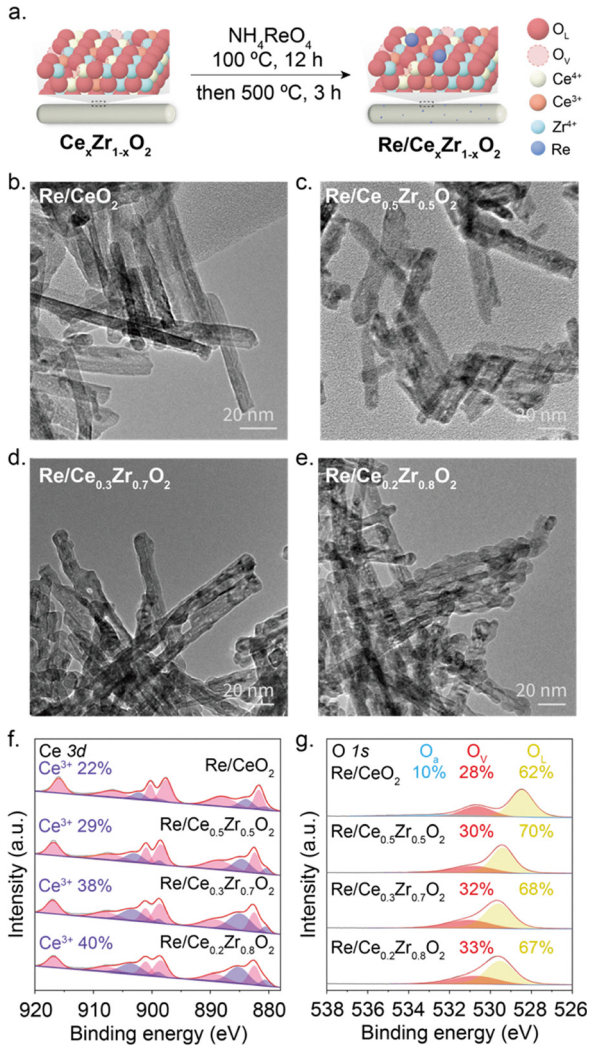

Fig. 3 Synthesis and characterization of $Re/Ce_xZr_{1-x}O_2$ catalysts. (a) Synthetic scheme for preparing $Re/Ce_xZr_{1-x}O_2$. TEM images of (b) Re/CeO_2, (c) $Re/Ce_{0.5}Zr_{0.5}O_2$, (d) $Re/Ce_{0.3}Zr_{0.7}O_2$, and (e) $Re/Ce_{0.2}Zr_{0.8}O_2$. (f) Ce 3d and (g) O 1s XPS spectra of the catalysts.

reduced $Ce_xZr_{1-x}O_2$ supports,[45,46] which possess higher O_V densities, to the supported Re species. This interpretation is further supported by the progressive reduction of the Re oxidation state with increasing Zr content (Fig. S3).

Powder X-ray diffraction (XRD) of the $Ce_xZr_{1-x}O_2$ nanorods showed a systematic shift of the (111) reflection toward higher 2θ values with increasing Zr content, consistent with lattice contraction arising from substitution of smaller Zr^{4+} ions (0.84 Å) for larger Ce^{4+} ions (0.97 Å). Correspondingly, the lattice parameter decreased from 5.40 Å (CeO_2) to 5.36 Å ($Ce_{0.3}Zr_{0.7}O_2$) (Table 1 and Fig. S4), confirming Zr incorporation into the fluorite lattice. In an inconsistent trend, however, $Ce_{0.2}Zr_{0.8}O_2$ exhibited a slightly lower diffraction angle than $Ce_{0.3}Zr_{0.7}O_2$ (Table 1, entries 3 and 4). This subtle lattice expansion indicates that $Ce_{0.2}Zr_{0.8}O_2$ no longer maintains a single solid solution, and the phase segregation has begun to occur, as further evidenced by the STEM-EDS mapping in Fig. 5(d).[47]

Table 1 Structural parameters of ceria–zirconia nanorod catalysts

		XRD		
Entry	Nanorod Catalysts	2θ (°)	d_{111} (Å)	a (Å)
1	CeO_2	28.60	3.117	5.400
2	$Ce_{0.5}Zr_{0.5}O_2$	28.74	3.103	5.374
3	$Ce_{0.3}Zr_{0.7}O_2$	28.82	3.094	5.359
4	$Ce_{0.2}Zr_{0.8}O_2$	28.78	3.098	5.366
5	Re/CeO_2	28.52	3.126	5.414
6	$Re/Ce_{0.5}Zr_{0.5}O_2$	28.72	3.105	5.377
7	$Re/Ce_{0.3}Zr_{0.7}O_2$	28.86	3.090	5.352
8	$Re/Ce_{0.2}Zr_{0.8}O_2$	28.70	3.107	5.381

Following rhenium impregnation, no noticeable shift in the (111) XRD reflection was detected, indicating that the Re species were dispersed on the surface rather than incorporated into the oxide lattice (Table 1, entries 5–8).[31] As shown in Fig. 3(f), the XPS spectra of $Re/Ce_xZr_{1-x}O_2$ exhibited a further increase in the Ce^{3+} fraction compared with the parent oxides, suggesting partial reduction of Ce^{4+} induced by the deposited Re species. Thus, although the bulk nanorod structure remained unchanged, the surface electronic environment became more reducible—an essential characteristic for facilitating Re redox cycling during catalysis.

The DODH activity of the $Re/Ce_xZr_{1-x}O_2$ catalysts was evaluated using dibutyl galactarate **1** in *n*-butanol, which served as both the reaction solvent and a green reductant (Fig. 4(a)). With 5 mol% Re loading, the desired *trans*, *trans*-muconic dibutyl ester **2** was obtained in yields ranging from 14% to 93% depending on the catalyst composition (Fig. 4(b)). Re/CeO_2 afforded a low yield of 14%, while $Re/Ce_{0.5}Zr_{0.5}O_2$ improved the yield to 32%. Notably, $Re/Ce_{0.3}Zr_{0.7}O_2$ delivered the highest yield of 93%, indicating that an optimal Ce/Zr ratio maximizes redox synergy between Ce^{3+} sites and rhenium species. The enhanced performance is attributed to the elevated Ce^{3+} reduced the yield fraction, which facilitates electron transfer to rhenium and accelerates the rate-determining $Re^{6+} \rightarrow Re^{4+}$ reduction in the DODH catalytic cycle. Further Zr enrichment ($Re/Ce_{0.2}Zr_{0.8}O_2$) resulted in a reduced yield of product **2** (24%), despite comparable Ce^{3+} concentrations and oxygen-vacancy levels. This observation suggests that excessive Zr incorporation disrupts effective Re–Ce interfacial communication. In this

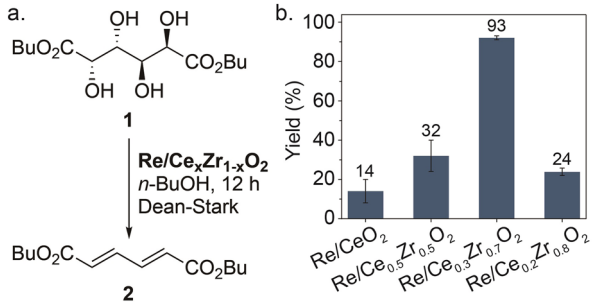

Fig. 4 (a) Reaction scheme for the $Re/Ce_xZr_{1-x}O_2$-catalyzed deoxydehydration (DODH) of dibutyl galactarate **1**. (b) Isolated yields of *trans*, *trans*-muconate **2** obtained over $Re/Ce_xZr_{1-x}O_2$ catalysts. Error bars represent standard errors.

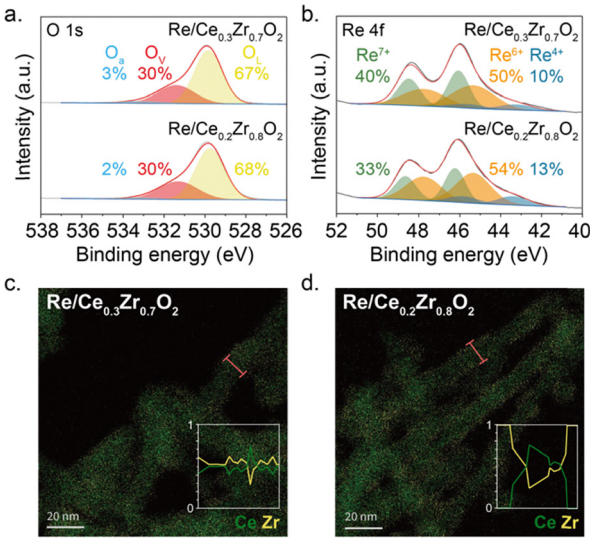

Fig. 5 Comparison of $Re/Ce_{0.3}Zr_{0.7}O_2$ and $Re/Ce_{0.2}Zr_{0.8}O_2$. XPS spectra of (a) O 1s and (b) Re 4f. STEM-EDS elemental mapping of (c) $Re/Ce_{0.3}Zr_{0.7}O_2$ and (d) $Re/Ce_{0.2}Zr_{0.8}O_2$.

case, a partially deoxydehydrated intermediate was also detected together with product **2** (Scheme S1).

Re 4*f* XPS spectra revealed a clear correlation between catalytic activity and the proportion of Re^{6+} species, which increased from 34% for Re/CeO_2 to 50% for $Re/Ce_{0.3}Zr_{0.7}O_2$ (Fig. S3). Interestingly, $Re/Ce_{0.2}Zr_{0.8}O_2$ exhibited the highest Re^{6+} fraction (54%) yet lower activity, suggesting that excessive Zr incorporation leads to electronic isolation of Re sites rather than effective redox coupling (Fig. 5(a) and (b)). Scanning transmission electron microscopy-energy dispersive spectroscopy (STEM-EDS) line profiles supported this interpretation: whereas $Re/Ce_{0.3}Zr_{0.7}O_2$ displayed a uniform Ce–Zr–Re distribution, $Re/Ce_{0.2}Zr_{0.8}O_2$ formed a ZrO_2-riched surface layer that impeded electron transfer between Re species and Ce^{3+} sites (Fig. 5(c) and (d)).

Collectively, these results demonstrate that controlled lattice engineering *via* a stepwise incorporation strategy leads to the formation of a $Ce_{0.3}Zr_{0.7}O_2$ solid solution through Zr diffusion into ceria nanorods. The resulting Zr-induced lattice strain and enhanced Ce^{3+} population promote lattice oxygen mobility. Subsequent incorporation of Re generates highly dispersed Re species on the nanorod surface, as confirmed by EDS elemental mapping (Fig. S5), thereby constructing a structurally integrated $Ce_{0.3}Zr_{0.7}O_2$ interface. At this interface, oxygen-vacancy-stabilized Re species enable efficient interfacial electron transfer, maximizing the Re–Ce redox synergy. This structural tuning enhances the reducibility of the catalytic interface and boosts DODH performance, whereas excessive Zr loading leads to electronic decoupling and diminished catalytic activity.

Conclusions

In summary, zirconium incorporation into ceria nanorods was systematically tuned to enhance the performance of rhenium catalysts for the deoxydehydration (DODH) of biomass-derived C_6 polyols. Introducing up to 70 at% Zr^{4+} induced lattice contraction, increased the Ce^{3+} fraction, and improved the reducibility of the mixed oxide, thereby strengthening redox coupling between Re species and Ce sites. The optimized $Re/Ce_{0.3}Zr_{0.7}O_2$ catalyst delivered a 93% yield of *trans*, *trans*-muconate from galactarate under mild conditions using *n*-butanol as a green reductant. These findings establish a clear relationship between lattice strain, oxygen-vacancy formation, and catalytic performance in Re-catalyzed DODH. Appropriate Zr incorporation effectively tunes the Ce–Zr lattice to promote electron transfer between Re and Ce^{3+} centers, enhancing redox efficiency. This lattice-engineering strategy provides a practical framework for designing mixed-oxide supports with tailored redox properties to enable selective and sustainable biomass conversion.

Author contributions

G. H. Y., H. S., and J. P. carried out the organic reactions. H. C., H. S., G. Y., and A. J. synthesized the catalysts. The catalysts and experimental data were analysed by H. C., G. Y., Y. S., and D. Y. The manuscript was written by Y. S. and D. Y., who also designed the project. All authors have approved the final version of the manuscript.

Conflicts of interest

There are no conflicts to declare.

Data availability

All data is available in the main text or in the supplementary information (SI). The supplementary information contains detailed experimental procedures along with additional figures and tables related to catalyst characterization. See DOI: https://doi.org/10.1039/d5nh00816f.

Acknowledgements

This work was financially supported by the Yang-Young Foundation, Samyang Corporation of Korea, the National Research Foundation of Korea (RS-2024-00398065) (D. Y.) and the Research Center Program of the IBS (IBS-R006-D1) in Korea (D. Y).

References

1 J. Rios, J. Lebeau, T. Yang, S. Li and M. D. Lynch, *Green Chem.*, 2021, **23**, 3172–3190.
2 W. Yan, G. Zhang, J. Wang, M. Liu, Y. Sun, Z. Zhou, W. Zhang, S. Zhang, X. Xu, J. Shen and X. Jin, *Front. Chem.*, 2020, **8**, 185.
3 M. T. Musser, *Ullmann's Encyclopedia of Industrial Chemistry*, Wiley-VCH Verlag GmbH & Co. KGaA, Weinheim, 2000.

4 Adipic Acid Market Size, Share, Analysis and Forecast, 2025, https://www.chemanalyst.com/industry-report/adipic-acid-market-715, (accessed 14 November 2025).
5 A. Castellan, J. C. J. Bart and S. Cavallaro, *Catal. Today*, 1991, **9**, 237–254.
6 S. Van de Vyver and Y. Román-Leshkov, *Catal. Sci. Technol.*, 2013, **3**, 1465–1479.
7 J. C. J. Bart and S. Cavallaro, *Ind. Eng. Chem. Res.*, 2015, **54**, 1–46.
8 N. N. Tshibalonza and J.-C. M. Monbaliu, *Green Chem.*, 2020, **22**, 4801–4848.
9 M. Lang and H. Li, *ChemSusChem*, 2022, **15**, e202101531.
10 R. T. Larson, A. Samant, J. Chen, W. Lee, M. A. Bohn, D. M. Ohlmann, S. J. Zuend and F. D. Toste, *J. Am. Chem. Soc.*, 2017, **139**, 14001–14004.
11 D. R. Vardon, M. A. Franden, C. W. Johnson, E. M. Karp, M. T. Guarnieri, J. G. Linger, M. J. Salm, T. J. Strathmann and G. T. Beckham, *Energy Environ. Sci.*, 2015, **8**, 617–628.
12 J. H. Jang, J. T. Hopper, I. Ro, P. Christopher and M. M. Abu-Omar, *Catal. Sci. Technol.*, 2022, **13**, 714–725.
13 M. Shiramizu and F. D. Toste, *Angew. Chem., Int. Ed.*, 2013, **52**, 12905–12909.
14 X. Li, D. Wu, T. Lu, G. Yi, H. Su and Y. Zhang, *Angew. Chem., Int. Ed.*, 2014, **53**, 4200–4204.
15 A. L. Denning, H. Dang, Z. Liu, K. M. Nicholas and F. C. Jentoft, *ChemCatChem*, 2013, **5**, 3567–3570.
16 F. C. Jentoft, *Catal. Sci. Technol.*, 2022, **12**, 6308–6358.
17 L. Sandbrink, E. Klindtworth, H.-U. Islam, A. M. Beale and R. Palkovits, *ACS Catal.*, 2016, **6**, 677–680.
18 I. Meiners, Y. Louven and R. Palkovits, *ChemCatChem*, 2021, **13**, 2393–2397.
19 Y. Stöckl, F. Rominger, A. S. K. Hashmi and T. Schaub, *ChemCatChem*, 2025, **17**, e202402010.
20 S. Mine, K. W. Ting, L. Li, Y. Hinuma, Z. Maeno, S. M. A. H. Siddiki, T. Toyao and K.-I. Shimizu, *J. Phys. Chem. C*, 2022, **126**, 4472–4482.
21 J. Lin, H. Song, X. Shen, B. Wang, S. Xie, W. Deng, D. Wu, Q. Zhang and Y. Wang, *Chem. Commun.*, 2019, **55**, 11017–11020.
22 K. W. Ting, S. Mine, A. Ait El Fakir, P. Du, L. Li, S. M. A. H. Siddiki, T. Toyao and K.-I. Shimizu, *Phys. Chem. Chem. Phys.*, 2022, **24**, 28621–28631.
23 F. M. Harth, M. Gabrič, J. Teržan, B. Hočevar, S. Gyergyek, B. Likozar and M. Grilc, *Catal. Today*, 2024, **441**, 114879.
24 E. Aneggi, D. Wiater, C. de Leitenburg, J. Llorca and A. Trovarelli, *ACS Catal.*, 2014, **4**, 172–181.
25 Tana, M. Zhang, J. Li, H. Li, Y. Li and W. Shen, *Catal. Today*, 2009, **148**, 179–183.
26 T. H. Vu, H.-R. An, P. T. Nguyen, J. Seo, C. Y. Kim, J.-I. Park, B. Son, H. Kim, H. U. Lee and M. I. Kim, *Nanoscale Horiz.*, 2025, **10**, 791–802.
27 Y. Nakagawa, S. Tazawa, T. Wang, M. Tamura, N. Hiyoshi, K. Okumura and K. Tomishige, *ACS Catal.*, 2018, **8**, 584–595.
28 D. Strauch, P. Weiner, B. B. Sarma, A. Körner, E. Herzinger, P. Wolf, A. Zimina, A. Hutzler, D. E. Doronkin, J.-D. Grunwaldt, P. Wasserscheid and M. Wolf, *Catal. Sci. Technol.*, 2024, **14**, 1775–1790.
29 D. Yan, X. Li, J. Zhong, Q. Ren, Y. Zeng, S. Gao, P. Liu, M. Fu and D. Ye, *Inorg. Chem.*, 2024, **63**, 11393–11405.
30 Z.-K. Han, W. Liu and Y. Gao, *JACS Au*, 2025, **5**, 1549–1569.
31 K. S. Vargas, J. Zaffran, M. Araque, M. Sadakane and B. Katryniok, *Mol. Catal.*, 2023, **535**, 112856.
32 M.-C. Tsai, T.-T. Nguyen, N. G. Akalework, C.-J. Pan, J. Rick, Y.-F. Liao, W.-N. Su and B.-J. Hwang, *ACS Catal.*, 2016, **6**, 6551–6559.
33 H.-X. Mai, L.-D. Sun, Y.-W. Zhang, R. Si, W. Feng, H.-P. Zhang, H.-C. Liu and C.-H. Yan, *J. Phys. Chem. B*, 2005, **109**, 24380–24385.
34 A. Chen, Y. Zhou, N. Ta, Y. Li and W. Shen, *Catal. Sci. Technol.*, 2015, **5**, 4184–4192.
35 S. Wei, Y. Zhao, G. Fan, L. Yang and F. Li, *Chem. Eng. J.*, 2017, **322**, 234–245.
36 W. Van Hoey, A. Rokicinska, M. Debosz, I. Majewska, P. Kustrowski and P. Cool, *Mater. Adv.*, 2024, **5**, 6983–6995.
37 R. Khatun, R. S. Pal, K. Bhati, A. C. Kothari, S. Singh, N. Siddiqui, S. Rana and R. Bal, *RSC Sustainability*, 2025, **3**, 844–855.
38 A. A. Alkhoori, O. Elmutasim, A. A. Dabbawala, M. A. Vasiliades, K. C. Petallidou, A.-H. Emwas, D. H. Anjum, N. Singh, M. A. Baker, N. D. Charisiou, M. A. Goula, A. M. Efstathiou and K. Polychronopoulou, *ACS Appl. Energy Mater.*, 2023, **6**, 8550–8571.
39 L. Li, P. Li, Y. Wang, L. Lin, A. H. Shah and T. He, *Appl. Surf. Sci.*, 2018, **452**, 498–506.
40 D. R. Mullins, S. H. Overbury and D. R. Huntley, *Surf. Sci.*, 1998, **409**, 307–319.
41 R. Eloirdi, P. Cakir, F. Huber, A. Seibert, R. Konings and T. Gouder, *Appl. Surf. Sci.*, 2018, **457**, 566–571.
42 B. M. Reddy, A. Khan, Y. Yamada, T. Kobayashi, S. Loridant and J.-C. Volta, *Langmuir*, 2003, **19**, 3025–3030.
43 B. M. Reddy, P. Bharali, P. Saikia, G. Thrimurthulu, Y. Yamada and T. Kobayashi, *Ind. Eng. Chem. Res.*, 2009, **48**, 453–462.
44 Y. Xi, W. Yang, S. C. Ammal, J. Lauterbach, Y. Pagan-Torres and A. Heyden, *Catal. Sci. Technol.*, 2018, **8**, 5750–5762.
45 F. Guo, J. Zhang, X. Hui, Y. Cao, P. He, H. Li, W. Zhou and L. Wang, *Nat. Commun.*, 2026, **17**, 1467.
46 A. Chutia, D. J. Willock and C. R. A. Catlow, *Faraday Discuss.*, 2018, **208**, 123–145.
47 J. Miao, N. Paudyal, R. V. Melinda and J. Zhou, *Catal. Sci. Technol.*, 2025, **15**, 7030–7042.

